JOURNAL OF AIRCRAFT
Vol. 29, No. 5, Sept.–Oct. 1992

Escape Strategies for Turboprop Aircraft in Microburst Windshear

Richard B. Bobbitt* and Richard M. Howard†
Naval Postgraduate School, Monterey, California 93943

A simulation was carried out on the performance of turboprop aircraft within a microburst windshear with the intent of providing specific flight procedures for optimal navigation through the disturbance. The windshear model used was a double-vortex-ring and point-source model duplicating the severe winds of the microburst encountered by Delta Airlines Flight 191 during an approach to landing at Dallas/Ft. Worth Airport on August 2, 1985. A parameter-estimation technique was used to vary the source strength and the vortices' strengths, sizes, and locations to best match the model-generated winds with those of the recorded low-level microburst windshear. Various escape strategies were tested using the flight performance characteristics of the U.S. Navy P-3 Orion and T-44 Pegasus turboprop aircraft during the flight phases of approach to landing, takeoff, and the low-altitude anti-submarine warfare mission. The results support a constant-pitch-angle escape procedure for all configurations and situations tested. The effects of changes in weight, wing loading, thrust-to-weight ratio, and takeoff rotation speed were treated, and stick control forces required to maintain pitch attitude with an immediate loss of airspeed were measured using the P-3 flight simulator.

Nomenclature

C_D = drag coefficient
C_{D0} = drag coefficient at zero deg angle of attack, referenced to the longitudinal axis of the aircraft
C_L = lift coefficient
C_{L0} = lift coefficient at zero deg angle of attack, referenced to the longitudinal axis of the aircraft
$C_{L\alpha}$ = lift curve slope, rad^{-1}
cg = center of gravity location
D = total drag, lbf
E = aircraft total energy, ft-lbf
E_s = specific energy, ft
g = gravitational constant, 32.174 ft/s^2
h = altitude above ground level (AGL), ft
K = induced-drag factor
L = total lift, lbf
m = aircraft mass, slugs
P_s = specific excess power, ft/s
Q = dynamic pressure, lbf/ft^2
q = pitch rate, rad/s
R_i = ith ring's radius
r = radial distance from z axis of vortex ring
r_i = ith ring's core radius
S = aircraft lift reference area, ft^2
T = thrust, lbf
t = time, s
V = equivalent airspeed, ft/s
V_{ref} = approach airspeed equating to 1.4 times power-off stall speed, KEAS
V_x = vortex-induced velocity component in x direction
V_y = vortex-induced velocity component in y direction
V_z = vortex-induced velocity component in z direction
V_1 = rotation airspeed, KEAS
V_2 = 50-ft target airspeed, KEAS
W = aircraft weight, lbf
W_h = vertical wind, ft/s
W_x = horizontal wind, ft/s
x = horizontal distance from the microburst center, ft
y = transverse distance from the microburst center, ft
z = vertical distance from the microburst center, ft
α = angle of attack, rad
γ_a = flight-path angle with respect to air mass, rad
θ = pitch angle, rad
κ = vortex-ring circulation, ft^2/s
λ = scaling term used in stream function approximation
ψ = vortex-ring stream function

Subscripts
g = ground-referenced system
i = image-referenced system; value for ith vortex ring
p = primary-referenced system

Superscript
$\cdot$ = time derivative

Introduction

THE microburst windshear has been identified as a serious threat to aircraft safety. Past investigations were often limited due to a lack of available flight data, but the current use of digital flight data recorders (DFDRs) provides sufficient information, along with air-traffic-control radar records, to extract the winds along the flight path.[1,2] Accurate modeling of identified microbursts, using the time history of the wind vectors, may then serve to provide realistic situations for microburst simulation and aircrew training.

Though many studies have been carried out on the potential effect of the microburst on the flight performance of airline transport aircraft, little work has been done related to windshear effects upon medium-to-lightweight turbopropeller aircraft. Military transport aircraft such as the C-130 are numerous and operate throughout the world. The U.S. Navy operates a fleet of P-3 Orion turboprop aircraft in all-weather, long-range patrol missions. Low-Level Wind Shear Alert Sys-

Received June 19, 1991; presented as Paper 91-2945 at the AIAA Flight Simulation Technologies Conference and Exhibit, New Orleans, LA, Aug. 12–14, 1991; revision received Sept. 11, 1991; accepted for publication Sept. 14, 1991.

*Graduate Student, Aeronautical Engineering Curriculum; Lieutenant Commander, U.S. Navy. Currently, Department Head, Patrol Squadron Forty-Seven, NASA, Moffett Field, CA.

†Assistant Professor, Department of Aeronautics and Astronautics. Senior Member AIAA.

tems (LLWSAS), currently in place at various airports around the country, serve to provide a warning of potential windshear to approaching and departing civilian air traffic, but no such information is available to military aircraft during low-level (200 ft above ground level [AGL]) patrol missions, or at remote military air bases.

This paper investigates the dynamic response of a P-3 aircraft and a light twin-engine turboprop during an encounter with a modeled low-level microburst windshear.

Microburst Model

Background

Fujita[3] first used the term "downburst" to describe a concentrated severe downdraft inducing an outward burst of high surface winds. The term "microburst" was used to define a downburst of horizontal extent of no more than 4 km. Early microburst models used to resolve large-scale effects involved the use of singularities of ideal fluid mechanics, such as sources or circular doublet sheets.[4] In many cases, simple downburst models can serve to accurately represent measured winds for particular windshear events.[5] Such models capture the general three-dimensional downburst wind behavior, yet in some cases may lack the ability to model the series of strong vertical wind gradients identified in recent data.

Caracena[6] suggested in 1982 that the airflow in a microburst may be structured as a vortex ring having downward circulation at the center. Various studies have made use of vortex-ring models to simulate the complex flowfield.[7-9] Schultz[10] developed a double-vortex-ring model which accurately simulated the microburst encounter of American Airlines Flight 539 (AA-539) at the Dallas/Ft. Worth Airport (DFW) on August 2, 1985. AA-539 traversed the microburst at an altitude of 2500 ft on a go-around, 110 s after Delta Airlines Flight 191 (DAL-191) encountered the microburst on final approach and contacted the ground about one mile short of the runway. Digital data from the two encounters of the same phenomenon have made this windshear event an important test case for microburst modeling. A generalized representation of the encountered microburst is shown in Fig. 1.

Model Development

A double-vortex-ring model was chosen to simulate the DAL-191 microburst windshear, following the development of such a model by Schultz[10] to represent the winds experienced by AA-539. A general description of the model will be given and the modifications noted.

A diagram of the two vortex rings and their image rings is shown in Fig. 2. The potential flow of the model is composed of vortex-ring filaments embedded in irrotational flow. The velocity components for each vortex were obtained by differentiating the vortex-ring stream function ψ

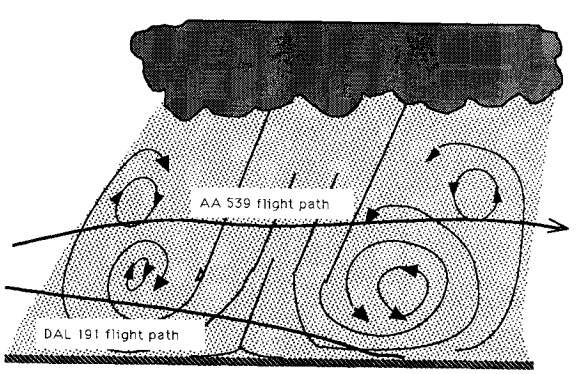

Fig. 1 Generalized microburst structure encountered at Dallas/Ft. Worth on August 2, 1985.

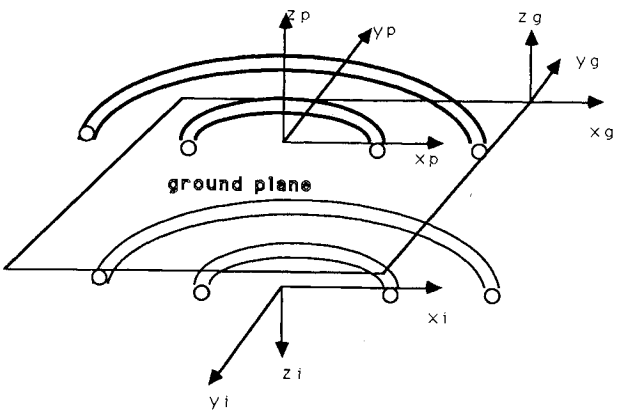

Fig. 2 Double-vortex-ring representation.

$$V_x = \frac{x}{r^2}\frac{\partial \psi}{\partial z} \tag{1}$$

$$V_y = \frac{y}{r^2}\frac{\partial \psi}{\partial z} \tag{2}$$

$$V_z = -\frac{1}{r}\frac{\partial \psi}{\partial r} \tag{3}$$

where r is the radial distance from the z axis

$$r = \sqrt{x^2 + y^2} \tag{4}$$

The stream function for a vortex-ring filament was obtained from the evaluation of an elliptic integral, an algebraic approximation for which is

$$\psi \simeq \frac{\kappa}{2\pi}(r_1 + r_2)\frac{0.788\,\lambda^2}{0.25 + 0.75\sqrt{1 - \lambda^2}} \tag{5}$$

where r_1 and r_2 represent the closest and farthest distances to the point of interest from the ring's filament; κ is the ring-filament strength; and λ is a scaling term used in the algebraic evaluation of the elliptic integral. Their algebraic relationships are

$$r_1 = \sqrt{z^2 + (r - R)^2} \tag{6}$$

$$r_2 = \sqrt{z^2 + (r + R)^2} \tag{7}$$

$$\lambda = (r_2 - r_1)/(r_2 + r_1) \tag{8}$$

where R is the radius of the filament.

Differentiating the stream function expression with respect to r and z gives

$$\frac{\partial \psi}{\partial r} = 0.788\delta_1(r_1 - r_2) - 0.394\lambda\delta_1(\eta_1 + \eta_2) + \delta_2[(\eta_1 - \eta_2) - \lambda(\eta_1 + \eta_2)] \tag{9}$$

$$\frac{\partial \psi}{\partial z} = \delta_1(0.788\sigma_2 - 0.394\lambda\sigma_1) + \delta_2(\sigma_2 - \lambda\sigma_1) \tag{10}$$

where η_1, η_2, σ_1, σ_2, δ_1, δ_2, and τ are defined

$$\eta_1 = (r + R)/r_2 \tag{11}$$

$$\eta_2 = (r - R)/r_1 \tag{12}$$

$$\sigma_1 = (z/r_2) + (z/r_1) \tag{13}$$

$$\sigma_2 = (z/r_2) - (z/r_1) \tag{14}$$

$$\delta_1 = (\kappa\lambda/\pi\tau) \tag{15}$$

$$\delta_2 = \frac{0.2955\kappa\lambda^3}{\pi\tau^2\sqrt{1-\lambda^2}} \tag{16}$$

$$\tau = 0.75\sqrt{1-\lambda^2} + 0.25 \tag{17}$$

The individual velocity components produced by each ring at a particular point in space can now be determined.

The viscous core of each ring is modeled by a continuous vorticity distribution based on a velocity damping factor devised by Schultz.[10] For more information on the basic model, see Ref. 10.

A parameter-estimation scheme was used to minimize the squared-error cost function based on the actual and modeled winds. The parameters of ring radius, ring core radius, position of the ring's center, and the ring's circulation were varied for both rings to achieve the best fit of the winds to those of the flight data.

In order to validate the programmed model before the modified case was considered, the original model was programmed and tested against the horizontal and vertical winds of the AA-539 encounter obtained by the methods of Ref. 2 as documented in Ref. 11. After confidence was gained in the modeling of the AA-539 event, modeling of the DAL-191 encounter then proceeded. The test-case results are shown in Fig. 3. Correlation with the vertical component is very good, but the headwind correlation fails to capture all of the strong gradients near the microburst center. Limitations exist in accurately predicting the horizontal component inside the small vortex ring. Future modifications can be attempted, as noted in Ref. 10. The crosswind component was not considered in this model; this component is not easily modeled by symmetric vortex rings,[10] and has much less impact on the aircraft behavior than the components in the vertical plane. Table 1 shows the final parameters representing the AA-539 windshear.

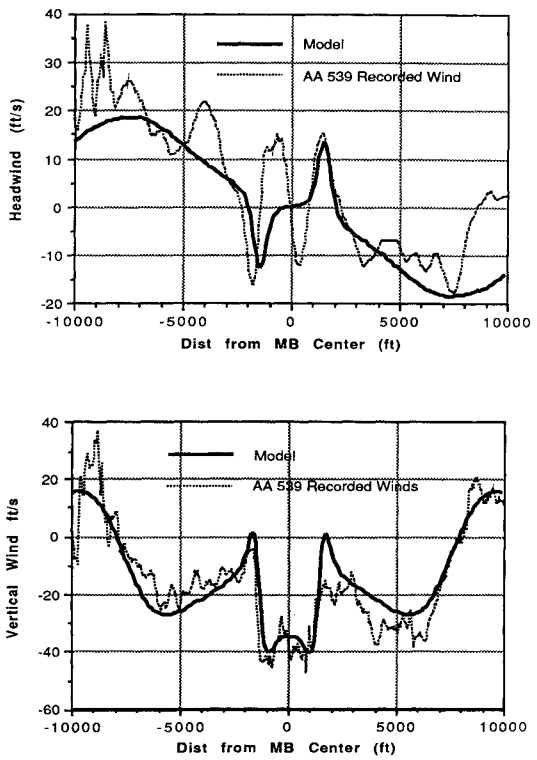

Fig. 3 Vortex-ring model comparison to recorded flight data (Schultz, Ref. 10).

Table 1 Windshear model parameters for AA-539 encounter at 2500 ft

Parameter	Large ring	Small ring
Ring radius, ft	8503.3	1701.7
Core radius, ft	2004.1	323.9
Ring circulation, ft²/s	431968.8	57204.9
x position, ft	0.0	50.0
y position, ft	3350.4	830.9
z position, ft	3400.6	2333.6

Table 2 Windshear model parameters for DAL-191 encounter near ground level

Parameter	Large ring	Small ring
Ring radius, ft	7000.0	1300.0
Core radius, ft	2004.1	323.9
Ring circulation, ft²/s	431968.8	131571.3
x position, ft	2500.0	300.0
y position, ft	−300.0	1.0
z position, ft	3400.6	800.0
x-dir. source strength, ft²/s	1355396	
z-dir. source strength, ft²/s	3049200	

Current Model

Due to the existence of high surface winds (outflow) in studied microbursts and the relative successes with stagnation-point and point-source models to capture this outflow, a point source and its image were added to the current double-vortex model simulating the microburst encountered by DAL-191. The point source was located at 10,000 ft above and below the ground plane, and the vertical and horizontal strengths were varied in a parameter-estimation scheme along with the ring parameters. The radial flow of the point source is represented by

$$V_r = (\Lambda/2\pi R_i) \tag{18}$$

where Λ is the source strength and R_i is the radial distance from the point source to the point of interest. The two sources contributed the following velocity components to those of the vortex rings:

$$V_{x_i} = V_{r_i}(x/R_i) \tag{19}$$

$$V_{z_i} = V_{r_i}(h/R_i) \tag{20}$$

The parameter-estimation method used an iterative process of varying each parameter individually, then calculating the total-system rms difference between the model and recorded winds. The 8 × 3 parameter matrix was refined after each successive iteration of the scheme until there was less than a 3% change in the total-system rms.

The results of matching the determined winds of the DAL-191 encounter are shown in Table 2 and in Figs. 4–6. Compared to the two rings in the AA-539 encounter, the small vortex ring is lower to the ground and displaced in the x direction. Compared to the total-system rms of 16 ft/s for the AA-539 model, the value for the current model for DAL-191 is 16.5 ft/s. Vertical and horizontal winds are shown in Fig. 4; the geometry of the modeled microburst is shown in Fig.

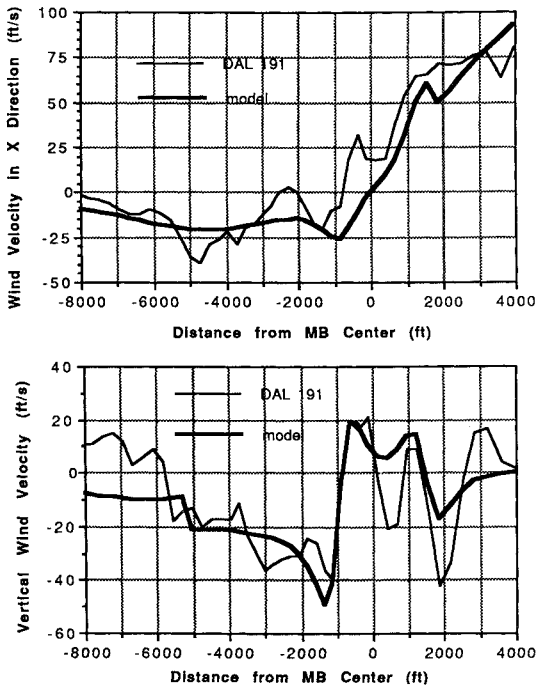

Fig. 4 DAL-191 recorded winds compared to winds of mathematical model.

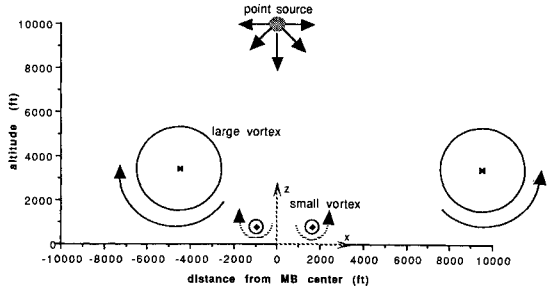

Fig. 5 Microburst model for DAL-191 encounter.

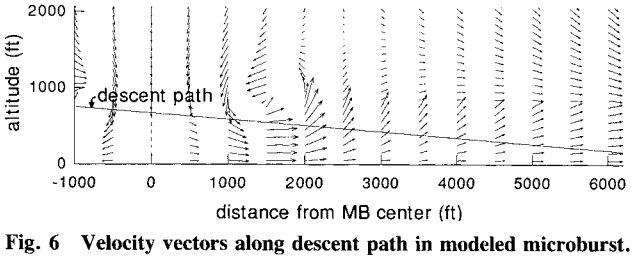

Fig. 6 Velocity vectors along descent path in modeled microburst.

5, and the velocity vectors of the flowfield along the desired descent path are shown in Fig. 6.

Aircraft Performance Modeling

The concept of aircraft specific energy was used to compare the flight trajectories of various windshear escape strategies. The total energy is defined as the sum of the airmass-relative kinetic energy and the inertial potential energy.

The relationship of the aircraft's motion through a moving airmass relative to the earth leads to the development of six coupled differential equations. The development is given in Ref. 12 and will not be included here. The equations of motion are

$$\dot{x} = V\cos\gamma_a + W_x \tag{21}$$

$$\dot{h} = V\sin\gamma_a + W_h \tag{22}$$

$$\dot{W}_x = \frac{\partial W_x}{\partial x}(\dot{x}) + \frac{\partial W_x}{\partial h}(\dot{h}) + \frac{\partial W_x}{\partial t} \tag{23}$$

$$\dot{W}_h = \frac{\partial W_h}{\partial x}(\dot{x}) + \frac{\partial W_h}{\partial h}(\dot{h}) + \frac{\partial W_h}{\partial t} \tag{24}$$

$$\dot{V} = \frac{T}{M}\cos\alpha - \frac{D}{M} - g\sin\gamma_a - \dot{W}_x\cos\gamma_a - \dot{W}_h\sin\gamma_a \tag{25}$$

$$\dot{\gamma}_a = \frac{T}{MV}\sin\alpha + \frac{L}{MV} - \frac{g}{V}\cos\gamma_a + \frac{\dot{W}_x}{V}\sin\gamma_a - \frac{\dot{W}_h}{V}\cos\gamma_a \tag{26}$$

The $\partial W_x/\partial t$ and $\partial W_h/\partial t$ terms were set equal to zero as a steady-state model was being considered. The equations are for a point-mass analysis in the vertical plane, and longitudinal dynamics are not considered. The lateral-directional response was not treated in this study.

The aircraft performance parameters of C_{L0}, $C_{L\alpha}$, C_{D0}, S, K, W, maximum thrust available, and maximum AoA were input into the equations of motion. C_L and C_D were determined from

$$C_L = C_{L0} + C_{L\alpha}\alpha \tag{27}$$

$$C_D = C_{D0} + K(C_L)^2 \tag{28}$$

The equations were solved using a second-order-accurate Euler predictor-corrector scheme with Richardson extrapolation.

Two aircraft were used to ascertain the resultant flight behavior to the DAL-191 microburst windshear. They were the U.S. Navy P-3 (Lockheed L-188) and the U.S. Navy T-44 (Beechcraft King Air H-90). The P-3 is a four-engine turboprop with gross weights from 75,000 to 135,000 lbs. The T-44 is a twin-engine turboprop in the light-twin transport category. For a more complete description of the aircraft, see Ref. 13.

Microburst Escape Strategies

Much work has been performed defining the optimal escape maneuvers for airline transport aircraft.[12,14–16] The Federal Aviation Administration (FAA) has generated an exhaustive Windshear Training Aid[17] aimed at enhancing the flight safety of modern transport aircraft. It addresses crew training requirements and suggests viable microburst escape strategies. If available, ground measurements indicating the existence of windshear will alert the transport aircraft in order to avoid an encounter.

As the P-3 aircraft rarely uses facilities equipped with windshear-warning instrumentation, the aircraft usually has no means of avoidance; it must rely solely on escape. The published guidelines[17] for microburst escape are based upon airline transport aircraft which vary significantly from the P-3. In this study, the results of flying different escape procedures are compared using the parameters of altitude, airspeed, and specific energy. Information from only those flight instruments available onboard the aircraft was considered in determining realistic response maneuvers. Though inertial navigation and true-airspeed computers provide flight-performance references through flight directors, the majority of the flight stations rely primarily on the basic flight instruments. These include the attitude indicator, airspeed indicator, altimeter, vertical-speed indicator, and angle-of-attack indicator. Three flight phases where a microburst encounter is critical were considered: the approach to landing, the takeoff, and the on-station phase. Results of the first two are presented here.

Approach to Landing

The landing approach scenario was based upon a descent to landing along a 3-deg glideslope. The microburst center was placed 10,300 feet from the end of the runway. The simulation started with the aircraft on glideslope 500 horizontal feet before the microburst center. This situation closely resembled the condition experienced by DAL-191. The aircraft was exposed to the windshear at $t = 0$ s, and the simulation continued for a set time or until ground impact occurred. The results presented here are for a P-3 at 89,500 lbs, a P-3 at 114,000 lbs, and a T-44. Additional test cases can be found in Ref. 13. Trim conditions were chosen for the given pitch angle and thrust to maintain a 3-deg glideslope at the target airspeed (V_{ref}). Pitch angle and thrust were maintained until a loss of airspeed equated to V_{ref} minus 20 knots. At that time, the aircraft performed one of the designated escape maneuvers.

Four microburst escape techniques were analyzed for the approach-to-landing encounter. They were:

1) *Constant airspeed*—Maximum thrust was applied and the pitch angle was set to 0 deg. This pitch angle was maintained until the airspeed equaled V_{ref}. Pitch angle was then adjusted to maintain the airspeed at $V_{ref} \pm 5$ knots.

2) *Constant altitude*—Maximum thrust was applied and a pitch angle set to obtain a positive rate of climb. Pitch angle was maintained until the target altitude (that at which the maneuver began) was established. Pitch angle was then adjusted to maintain the target altitude ± 20 ft.

3) *Constant pitch angle*—Maximum thrust was applied and a pitch angle set and maintained. Pitch angles of 5, 8, 10, and 15 deg were used.

4) *Constant angle of attack*—Maximum thrust was applied and the pitch angle was adjusted to obtain a given angle of attack. Angle-of-attack (AoA) values of 12, 15, and 20 units were used for the P-3 model.

Constraints applied to the escape maneuvers were a pitch-rate limit of 5 deg/s, a thrust application rate of 50% maximum thrust/s for the P-3, and a thrust application rate of 20% maximum thrust/s for the T-44. Maximum pitch angle was limited not to exceed maximum AoA.

Takeoff

The simulation began with the aircraft lifting off 1200 ft prior to the microburst center at the appropriate liftoff speed (V_1). Initial pitch angle was that required to achieve takeoff safety speed (V_2) at 50 ft. Maximum thrust was used for all takeoff simulations. The execution of the particular escape maneuver began when the rate of climb was less than zero, or the airspeed fell below V_2. Presented here are results for a P-3 at 120,000 lbs and a T-44.

Four escape methods were considered for the takeoff encounter. They were:

1) *Constant airspeed*—If the airspeed was less than V_2 at the initiation of the escape maneuver, pitch angle was reduced to 0 deg. If the airspeed was greater than V_2 at initiation, pitch angle was increased. In both cases, pitch angle was manipulated to maintain an airspeed of $V_2 \pm 5$ knots once V_2 was re-established.

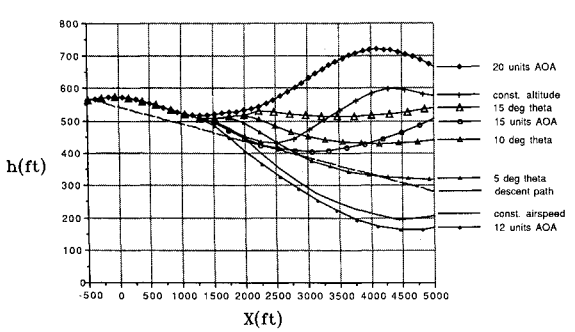

Fig. 7 Altitude results for microburst encounter, P-3, approach to landing, 89,000 lbs.

2) *Constant altitude*—Pitch angle was varied to maintain altitude ± 20 feet about the target altitude at which the escape maneuver began.

3) *Constant pitch angle*—Pitch angle was held constant throughout the maneuver. Values treated were 5, 10, and 15 deg.

4) *Constant angle of attack*—Pitch angle was varied to maintain a constant AoA value.

For the above maneuvers, a pitch rate of 5 deg/s was used and maximum thrust maintained. Pitch angle was reduced whenever critical AoA was exceeded.

Results

Approach to Landing

To validate the model, a three-engine heavy airline transport model was flown through the microburst and compared to the results of the DAL-191 flight. Inputs to the aircraft control were the recorded pitch angle and thrust of the DAL-191 records.[11] The flight-path results were almost identical down to the point of ground impact. The comparison of altitude, airspeed, and angle of attack can be found in Ref. 13.

Figures 7–9 depict the response for different escape maneuvers executed by a P-3 at 89,000 lbs gross weight as it flew through the microburst. Plots of altitude, velocity, and specific

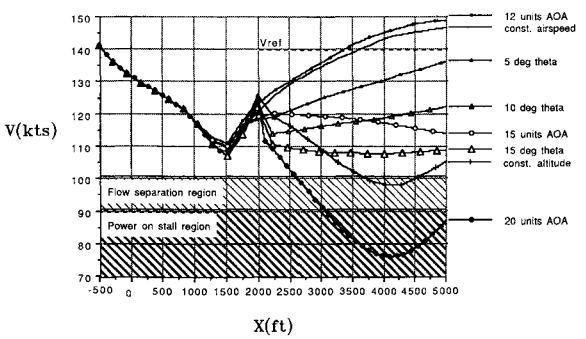

Fig. 8 Airspeed results for microburst encounter, P-3, approach to landing, 89,000 lbs.

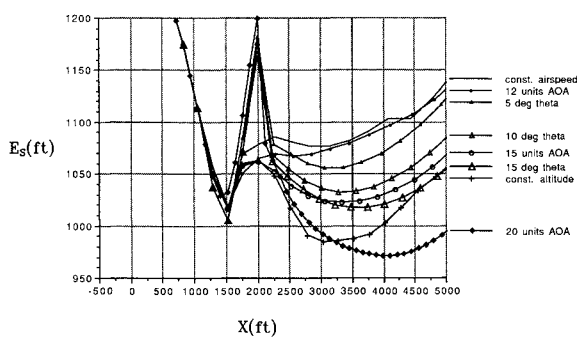

Fig. 9 Specific energy results for microburst encounter, P-3, approach to landing, 89,000 lbs.

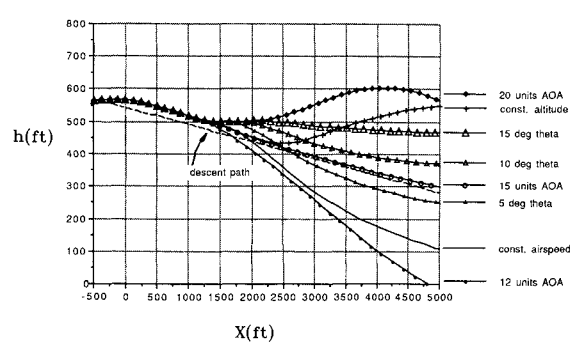

Fig. 10 Altitude results for microburst encounter, P-3, approach to landing, 114,000 lbs.

energy are shown for all cases. The constant-airspeed and 12-units AoA maneuvers were rejected due to resulting flight trajectories below the descent path, as can be seen in Fig. 7. The 20-units AoA and constant-altitude maneuvers were rejected due to resulting speeds below that for flow-separation, as can be noted in Fig. 8. (Maximum lift coefficient was not included in the simulation of the escape strategies.) Figure 9 indicates the 5-deg pitch-angle criterion resulted in the highest specific energy value at 5000 ft past the microburst center, followed by the 10-deg pitch-angle maneuver.

The next three figures depict the results obtained for different escape maneuvers executed by a P-3 at 114,000 lbs gross weight. As can be noted in Fig. 10, the 12-units AoA, constant-airspeed, and 5-deg pitch-angle maneuvers were rejected due to trajectories below the desired descent path (the 12-unit AoA strategy resulted in ground impact at 4800 ft). As seen in Fig. 11, the 20-units AoA and constant-altitude cases resulted in airspeeds into the power-on stall region, while the 15-deg pitch angle maneuver gave an airspeed at x = 5000 ft slightly into the flow-separation region. Specific results shown in Fig. 12 indicate that of the remaining strategies, the 15-units AoA and 10-deg pitch angle maneuvers gave the highest values of total energy height.

For both weights of the P-3, of the maneuvers not rejected for low altitude or airspeed, the 10-deg pitch angle strategy achieved a high value of specific energy. Of those not rejected, the 10-deg pitch angle resulted in the highest value of altitude.

The approach-to-landing phase through the microburst windshear was computed for the T-44 aircraft. As seen in Fig. 13, the 10-units AoA, constant-airspeed, and 16-units AoA escape maneuvers resulted in trajectories below the descent path. The 25-units AoA and constant-altitude maneuvers were subsequently rejected due to low airspeeds as can be seen in Fig. 14. Energy plots in Fig. 15 show the remaining maneuvers, in decreasing order of success, to be the 5, 10, and 15-deg pitch-angle strategies. Large variances in altitude or airspeed between these strategies result in relatively small changes in terms of specific energy.

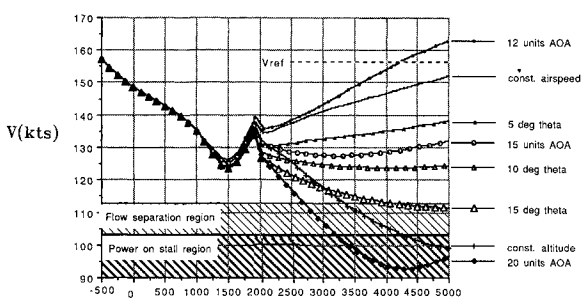

Fig. 11 Airspeed results for microburst encounter, P-3, approach to landing, 114,000 lbs.

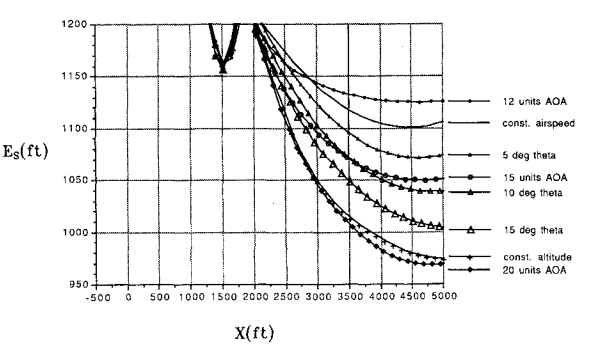

Fig. 12 Specific energy results for microburst encounter, P-3, approach to landing, 114,000 lbs.

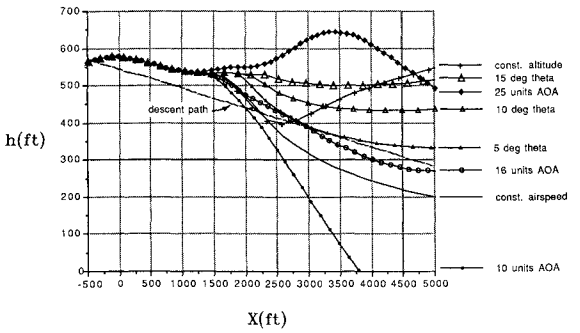

Fig. 13 Altitude results for microburst encounter, T-44, approach to landing.

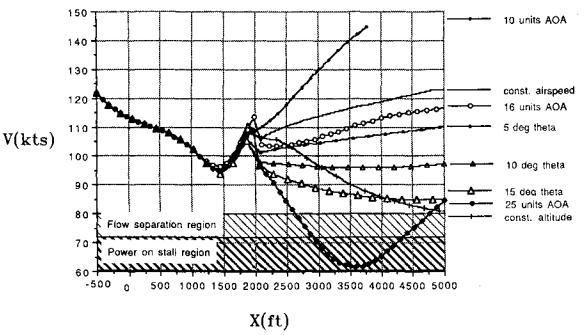

Fig. 14 Airspeed results for microburst encounter, T-44, approach to landing.

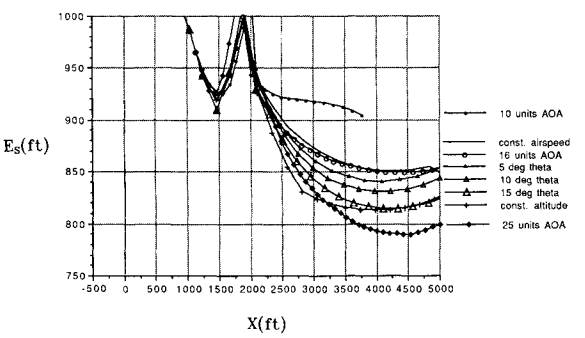

Fig. 15 Specific energy results for microburst encounter, T-44, approach to landing.

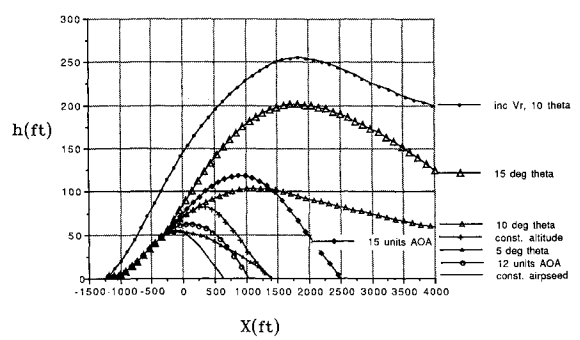

Fig. 16 Altitude results for microburst encounter, P-3, takeoff, 120,000 lbs.

Takeoff Phase

Takeoff escape strategies were evaluated for the P-3 at 120,000 lbs and for the T-44. Again, plots of altitude, airspeed, and specific energy are shown.

Figure 16 shows that the strategies of constant airspeed, constant altitude, 5-deg pitch angle, 12-units AoA, and 15-units AoA all result in ground impact between 500 and 2500 ft of the takeoff point. The 10-deg and 15-deg pitch-angle

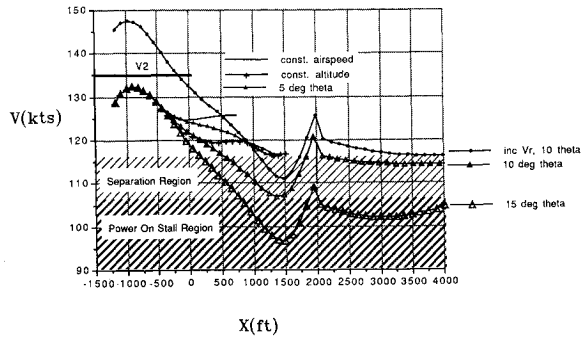

Fig. 17 Airspeed results for microburst encounter, P-3, takeoff, 120,000 lbs.

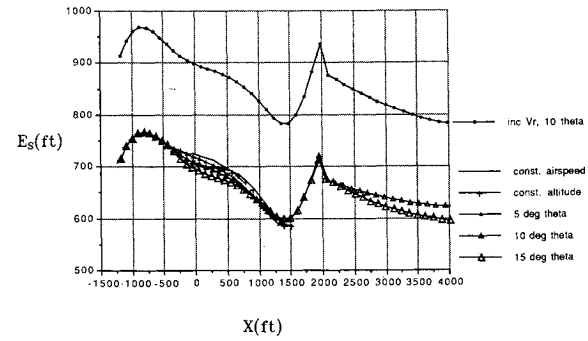

Fig. 18 Specific energy results for microburst encounter, P-3, takeoff, 120,000 lbs.

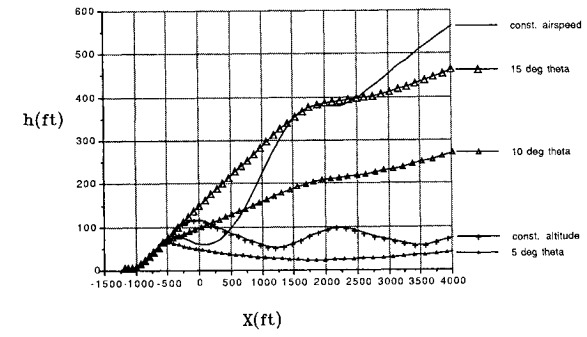

Fig. 19 Altitude results for microburst encounter, T-44, takeoff.

maneuvers result in a survival of the encounter; the 15-deg pitch-angle maneuver results in a higher altitude at 4000 feet from the microburst center, but the 10-deg pitch-angle strategy has a flatter descent slope. Figure 17 indicates that neither maneuver results in an airspeed above that for completely attached flow over the wing. The 10-deg pitch-angle case results in an airspeed slightly slower than that for the onset of flow separation, while the 15-deg pitch-angle case is deep within the power-on stall region. The specific energy of the remaining two strategies, as shown in Fig. 18, are almost identical, with the 10-deg case slightly higher.

Included with the P-3 test data at 120,000 lbs is the resulting flight performance when the rotation speed, V_1, is increased 18 knots at the liftoff point, 1200 feet before the microburst center, for the 10-deg pitch-angle case. The greatest benefit seen from this increase in liftoff speed is an increase in altitude. There is a maximum height gain of 140 ft over that for the standard 10-deg pitch-angle case—an increase of over 200%. The increase in specific energy is 25% over that for the standard 10-deg pitch-angle case. This is significantly greater than the spread of specific energy values between the other escape maneuvers. However, the airspeed of the increased-rotation-speed maneuver is only 5 knots above that for the standard case. This result shows that the additional speed at rotation translates to increased altitude.

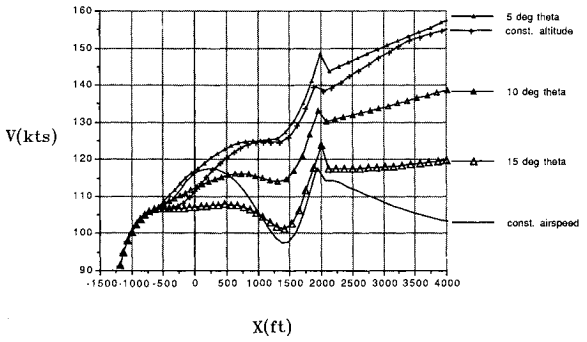

Fig. 20 Airspeed results for microburst encounter, T-44, takeoff.

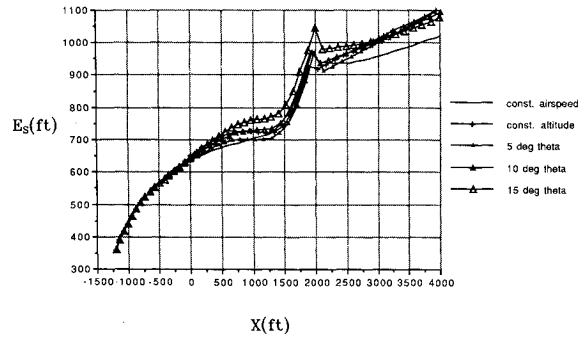

Fig. 21 Specific energy results for microburst encounter, T-44, takeoff.

The next three figures consider the response of the T-44 aircraft to a takeoff microburst encounter. As indicated in Fig. 19, all escape maneuvers resulted in ground clearance at 4000 feet horizontal distance beyond the microburst center. The tradeoff of airspeed for altitude is noted in Fig. 20. Here, the escape-maneuver order is reversed from that of the previous figure. The 10-deg and 15-deg pitch-angle maneuvers result in moderately increasing values of both altitude and airspeed 4000 ft from the microburst center, and appear to be favorable recommendations for optimal escape strategies. Specific energies for the maneuvers are shown in Fig. 21. Values are almost identical for all escape maneuvers.

Other Cases

Various other flight conditions were treated. These can be found in Ref. 13 and will only be briefly mentioned. A P-3 flying at its maximum takeoff gross weight of 135,000 lbs failed to achieve a successful takeoff regardless of the escape maneuver attempted. A P-3 in the approach-to-landing phase at 89,500 lbs operating on three of its four engines resulted in a response similar to that for the heavier P-3. An analysis of the 120,000-lb P-3 during loiter operations resulted in a successful on-station microburst encounter. Additional thrust was not applied until a loss of 40 knots occurred. The P-3 navigated the encounter with an altitude deviation no greater than ± 20 ft and a pitch-angle input no greater than 10 deg.

In a comparison of the effects of aircraft weight, wing loading, and thrust-to-weight ratio, it was found that an increased thrust-to-weight ratio decreased the effect of the windshear (as expected) and a light wing loading allowed for a more immediate transfer of energy. Weight as an independent parameter was found to be irrelevant.

Stick Force for Off-Trim Airspeed

The expected change in flight control "feel" for the P-3 aircraft is light; flight tests indicate that the stick-force gradient is shallow for this aircraft.[18] In the takeoff/approach-flap configuration, at an aft cg of 29% mean aerodynamic chord (MAC), a stick force of 11 lbs is required for a 30-knot decrease from trim airspeed. Stick force increases to a 16-lb

pull with the most forward cg of 16% MAC. Flight test data indicate that stick forces are expected to be almost identical for the approach-to-landing and takeoff microburst-encounter flight phases.

The P-3 Flight Simulator was used to confirm the results relating to off-speed stick force expected during a microburst encounter. The simulator allows one or more flight parameters to be frozen. For the test case, the altitude was frozen at 500 feet and the aircraft was trimmed with maximum power at the reference airspeed. The airspeed was then reset and frozen to the lower airspeed value expected during a microburst windshear. The control force required to maintain a pitch attitude was then measured. With maximum power applied and with a 10-deg pitch attitude, the stick force ranged from a 6-lb pull with an aft cg to a 24-lb pull with a forward cg.

Conclusions

Using the available instruments on board the P-3 and T-44 aircraft, the optimal escape procedure was found to be flying a constant value of pitch angle. Constant AoA maneuvers sometimes resulted in superior performance, but use of AoA indicators is not recommended due to expected instrument-lag errors during turbulent conditions, and to the fact that AoA indication is seldom used during the approach phase.

Pitch-angle values from 5 to 15 deg were identified as optimal for the approach-to-landing encounter. A pitch-angle value of 10 deg is felt to provide suitable recovery for the P-3 as configured in the study. A 10-deg pitch angle was also found to work well for the T-44 in the approach-to-landing phase. In the takeoff encounter, a pitch angle of 15 deg was found to work best for the T-44.

Recommendations for the approach-to-landing phase for the P-3 are to set and maintain maximum power while setting a 10-deg pitch attitude. For the takeoff encounter, if indications warrant the potential of windshear, rotation speed should be increased to 140 knots and a pitch attitude of 10 deg maintained.

The optimum escape procedures are identical for all gross weights. The approach-to-landing escape procedure is identical for three or four operating engines.

The airspeed will decay rapidly and remain abnormally low during a microburst penetration. An elevator force of 5–10 lbs can be expected to maintain a 10-deg pitch attitude with full power for the P-3. Flight tests have indicated that the P-3 has no unusual short-period, phugoid, or cross-couple dynamics which would alter these recommendations.

The only different recommendation for the T-44 is the 15-deg pitch angle for takeoff. Takeoff and approach-to-landing flap configurations differ for the T-44, while the P-3 has an identical flap setting for the landing and takeoff flight phases.

In summary, the flight responses of two Navy turboprop aircraft were studied for optimal escape strategies in the event of microburst penetration. The microburst modeled was that encountered by DAL-191 at DFW Airport on August 2, 1985. Improved modeling of measured microbursts such as DAL-191 will contribute to the ability to provide accurate simulation for enhanced aircrew training and aircraft safety.

References

[1]Bach, R. E., Jr., and Wingrove, R. C., "Analysis of Windshear from Airline Flight Data," *Journal of Aircraft*, Vol. 26, No. 2, 1989, pp. 103–109.

[2]Wingrove, R. C., and Bach, R. E. Jr., "Severe Winds in the Dallas/Ft. Worth Microburst Measured from Two Aircraft," *Journal of Aircraft*, Vol. 26, No. 3, 1989, pp. 221–224.

[3]Fujita, T. T., "Spearhead Echo and Downburst Near the Approach End of a John F. Kennedy Airport Runway, New York City," Univ. of Chicago, SMRP Res. Paper 137, Chicago, IL, 1976.

[4]Zhu, S., and Etkin, B., "Model of the Wind Field in a Downburst," *Journal of Aircraft*, Vol. 22, No. 7, 1985, pp. 595–601.

[5]Oseguera, R. M., and Bowles, R. L., "A Simple, Analytic 3-Dimensional Downburst Model Based on Boundary Layer Stagnation Flow," NASA TM-100632, July 1988.

[6]Caracena, F., "Is the Microburst a Large Vortex Ring Imbedded in a Thunderstorm Downdraft?," *EOS Trans. Amer. Geophys. Union*, Vol. 63, 1982, p. 89.

[7]Ivan, M., "A Ring-Vortex Downburst Model for Flight Simulations," *Journal of Aircraft*, Vol. 23, No. 3, 1986, pp. 232–236.

[8]Swolinsky, M., "Wind Shear Models for Aircraft Hazard Investigation," AGARD CP-470, May 1989, pp. 2-1 to 2-17.

[9]Grantham, W. J., Roetcisoender, G. G., and Parks, E. K., "DFW Microburst Model Based on AA-539 Data," *Journal of Aircraft*, Vol. 27, No. 11, 1990, pp. 917–922.

[10]Schultz, T. A., "A Multiple-Vortex-Ring Model of the DFW Microburst," AIAA Paper 88-0685, Jan. 1988.

[11]"Aircraft Accident Report, Delta Airlines, Inc., Lockheed 1-1011-385-1, N726D, Dallas/Fort Worth International Airport, Texas, August 2, 1985," National Transportation Safety Board, Rept. AAR-86/05, Washington, DC, Aug. 1986.

[12]Hinton, D. A., "Flight-Management Strategies for Escape From Microburst Encounters," NASA TM-4057, Aug. 1988.

[13]Bobbitt, R. B., "Escape Strategies for Turboprop Aircraft in a Microburst Windshear," Masters Thesis, Naval Postgraduate School, Monterey, CA, March 1991.

[14]Bray, R. S., "Aircraft Performance and Control in Downburst Wind Shear," Society of Automotive Engineers Paper 861698, 1986.

[15]Robinson, P. A., and Reid, L. D., "Modeling of Turbulence and Downbursts for Flight Simulators," *Journal of Aircraft*, Vol. 27, No. 8, 1990, pp. 700–707.

[16]Psiaki, M. L., and Stengel, R. F., "Optimal Aircraft Performance During Microburst Encounter," *Journal of Guidance, Control, and Dynamics*, Vol. 14, No. 2, 1991, pp. 440–446.

[17]"Windshear Training Aid," Federal Aviation Administration, National Archives, Washington, DC, 1987.

[18]"Lockheed P3V-1 Flying Qualities," Lockheed Aircraft Corp. Rept. 13133, Nov. 19, 1959.